Arabian Journal of Chemistry (2016) 9, S1847–S1857

King Saud University

Arabian Journal of Chemistry

www.ksu.edu.sa
www.sciencedirect.com

ORIGINAL ARTICLE

Synthesis, spectroscopic investigation and antimicrobial activities of some transition metal complexes of a *[(2-hydroxyacetophenone)-3-isatin]-bishydrazone*

S.S. Swathy [a], R. Selwin Joseyphus [b], V.P. Nisha [a], N. Subhadrambika [a], K. Mohanan [a,*]

[a] *Department of Chemistry, University of Kerala, Kariavattom Campus, Trivandrum 695 581, India*
[b] *Department of Chemistry, St. John's College, Anchal, Kollam 691 306, Kerala, India*

Received 14 February 2012; accepted 26 May 2012
Available online 2 June 2012

KEYWORDS

Bishydrazone;
IR;
EPR;
Antimicrobial activity;
Corrosion inhibition

Abstract A bishydrazone was obtained by the condensation of isatin monohydrazone with 2-hydroxyacetophenone, which formed a series of complexes with manganese(II), cobalt(II), nickel(II), copper(II) and zinc(II). The ligand and the metal complexes were characterized on the basis of elemental analysis, molar conductance, magnetic moment, IR, UV–Visible, mass, ^{1}H NMR, EPR, and thermal analysis. Spectral studies revealed that the ligand acted as monobasic tridentate, coordinating to the metal ion through the deprotonated phenolate oxygen, azomethine nitrogen and carbonyl oxygen atom of the isatin moiety. The low molar conductance values indicate that all complexes are non-electrolytes. Based on the spectral results and magnetic susceptibility measurements, suitable geometry was proposed for each complex. The EPR spectral data indicated that metal–ligand bond had considerable covalent character. The ligand and its nickel(II) complex were subjected to XRD studies. Thermal decomposition study of nickel(II) complex was also carried out. *In vitro* biological screening effects of the compounds were tested against the bacteria and the fungal species by the agar disc diffusion method. A comparative study of the MIC values of the ligand and its complexes indicated that the copper(II) complex exhibited higher antimicrobial activity than the free ligand. The corrosion inhibitory activity of the ligand and its nickel(II) complex used in acid (H_2SO_4) media was also examined by weight loss measurements.

* Corresponding author. Tel.: +91 9447696794.
E-mail addresses: rajendran.biju@gmail.com (S.S. Swathy), drkmohanan@rediffmail.com (K. Mohanan).

Peer review under responsibility of King Saud University.

Production and hosting by Elsevier

http://dx.doi.org/10.1016/j.arabjc.2012.05.004

1. Introduction

Hydrazones form an interesting class of chelating ligands which contain an azomethine group linked to a nitrogen atom and find extensive application in various fields (Mariar et al., 2004; Sridhar and Ramesh, 2001). The coordination behaviour of hydrazones depends on pH of the medium, nature of the substituent and position of hydrazone group relative to other nucleus. Although metal complexes of monohydrazones derived from isatin have been extensively investigated, those formed from bishydrazones have received comparatively less attention so far (Sridhar et al., 2001; Murukan and Mohanan, 2007; Hassan, 1997). 2-Hydroxyacetophenone is a versatile chemical intermediate with significant commercial applications (Mohanan et al., 2008). The compounds containing isatin moiety possess interesting biological and pharmacological activities (Ercag et al., 2006; Pandeya et al., 1999; Sridhar et al. 2002). In this paper, we report the synthesis, structural characterization, thermal decomposition, antimicrobial and corrosion inhibitory activities of some transition metal complexes with the host of a bishydrazone derived from isatin monohydrazone and 2-hydroxyacetophenone *viz*. (L = *[(2-hydroxyacetophenone)-3-isatin]-bishydrazone)*.

2. Experimental

2.1. Materials

All chemicals used were of analytical grade. Isatin, hydrazine hydrate (99%) and 2-hydroxy acetophenone were obtained from Fluka and Sisco Chemicals.

2.2. Synthesis of ligand

2.2.1. Synthesis of monohydrazone

Isatin (1.47 g, 10 mmol) dissolved in MeOH (40 mL) and was added to a solution of hydrazine hydrate (0.5 mL, 10 mmol) dissolved in hot MeOH (10 mL). The resulting solution was refluxed for 3 h on a waterbath and the yellow coloured compound was separated out on cooling. It was filtered, dried in vacuum and further purified by recrystallization from methanol (m.p. 226 °C; yield ~95%).

2.2.2. Synthesis of bishydrazone

2-Hydroxyacetophenone (0.6 mL, 5 mmol) dissolved in MeOH (10 mL) was added to a solution of isatin monohydrazone (0.80 g, 5 mmol) in hot MeOH (70 mL). The resulting mixture was refluxed on a waterbath for 4 h. The volume of the solution was reduced to about 50 mL and allowed to cool at room temperature. The orange coloured compound separated out was filtered, washed with MeOH and dried in vacuum (m.p. 235 °C; yield ~83%).

2.3. Synthesis of metal complexes

2.3.1. Manganese(II) complex (M:L = 1:2)

To a methanolic solution of ligand (0.28 g, 1 mmol) a solution of manganese(II) acetate (0.12 g, 0.5 mmol) in MeOH (10 mL) was added in small portions with constant stirring. The reaction mixture was then refluxed on a water bath for 5 h and then cooled to room temperature. The pH of the solution was adjusted to ~7 using alcoholic ammonia solutions (buffer solution). The complex separated was filtered, washed with MeOH and then dried in vacuum.

2.3.2. Cobalt(II) complex

Cobalt(II) complex (M:L = 1:2) was synthesized according to the procedure similar to that followed for manganese(II) complex, except the refluxing time was about 4 h and the pH was maintained at ~6. The solid product was filtered off, washed several times with MeOH and dried in vacuum.

2.3.3. Nickel(II) complex

Nickel(II) complex (M:L = 1:1) was prepared by adopting the procedure for the preparation of cobalt(II) complex, except that the pH was maintained at ~6.5. On adding the nickel(II) chloride, the ligand solution turned to light brown colour. The reaction mixture was refluxed for 3 h. The product obtained was filtered, washed with MeOH and dried in vacuum.

2.3.4. Copper(II) complex

For the synthesis of copper(II) complex (M:L = 1:1) the above mentioned preparative method was followed, except that the refluxing time was about 2 h. The pH of the solution was maintained between 6.5 and 7.5. The reaction mixture was then reduced to half of its original volume and kept overnight. The complex separated out was filtered, washed with MeOH and dried in vacuum.

2.3.5. Zinc(II) complex (M:L = 1:1)

A solution of zinc(II) chloride (0.14 g, 1 mmol) in methanol(15 mL), was added gradually in small amounts to a hot solution of ligand (0.28 g, 1 mmol) in MeOH (60 mL). The pH of the solution was maintained at ~7.5 and refluxed for about 6 h. The product obtained was filtered, washed with MeOH and dried in vacuum.

2.4. Physical measurements

Elemental analysis (C, H and N) was carried out using a Heracus Carlo Erba 1108-CHN Analyzer. The metal contents in the complexes were analysed using an atomic absorption spectrometer (GBC Avanta). The electronic spectra were recorded on Hitachi 320 UV–Vis spectrometer in the range 200–900 nm. Infrared spectra of the ligand and the metal complexes were recorded on a Jasco FTIR-410 spectrometer using KBr pellets and far infrared in the 500–100 cm^{-1} region using CsI-discs on a polytech FIR 30 Fourier spectrometer. Proton NMR spectra of the ligand and its zinc(II) complex were recorded in DMSO-d_6 on a JEOL GSX 400 NB 400 MHz FT-NMR spectrometer. FAB-mass spectra of the ligand and its nickel(II) complex were recorded on a JEOL SX102/DA-6000 mass spectrometer/data system using Argon/Xenon (6 kV, 10 mA) as the FAB gas. The accelerating voltage was 10 kV and the spectrum recorded at room temperature using m-nitrobenzoylalcohol as the matrix. Molar conductance measurements were conducted using 10^{-3} M solution of the complexes in DMSO at room temperature with a Systronics model 304 digital conductivity meter. Magnetic measurements of the metal complexes were performed on a Magway MSB Mk_1 magnetic susceptibility balance. The EPR spectrum of the copper(II) complex was recorded using a Varian E-112 EPR spectrometer. The

thermogravimetric analysis of the nickel(II) complex was carried out using a thermobalance of the type Mettler Toledo System in dynamic air. The XRD patterns of the ligand and its nickel(II) complex were recorded on a Rigaku D_{max} X-ray diffractometer using Cu Kα radiation (λ = 1.5404 Å).

2.5. In vitro antimicrobial activity

The *in vitro* antimicrobial activity of the ligand and its complexes were tested against the bacterial species, *Staphylococcus aureus, Escherichia coli* and *Salmonella typhi*, and the fungal species *Rhizopus stolonifer* and *Candida albicans* by agar disc diffusion method (Bauer et al., 1996). Streptomycin and Nystatin were used as standards for antibacterial and antifungal agents. The standard samples of antimicrobial activity are done at 100 μg/ml concentration in DMSO. The test organisms were grown on nutrient agar medium in petri plates. The antibacterial and antifungal activities of the ligand and its metal complexes were done at 50, 100 and 200 μg/ml concentration in DMSO solvent by the minimum inhibitory concentration (MIC) method. The discs were placed on the previously seeded plates and incubated at 37 °C. The diameter of inhibition zone around each disc was measured after 24 h for bacterial and 72 h for fungal species. Activity was determined by measuring the diameter of the zone showing complete inhibition (mm).

2.6. Corrosion

2.6.1. Corrosion weight loss determination

The pretreated coupons were weighed and suspended vertically for 15 days in 100 mL aerated, unstirred 1 M H_2SO_4 with and without the corrodent-inhibitor of different concentrations varying from 1×10^{-3} g to 5×10^{-3} g. The coupons were then removed and washed with 20% NaOH solution containing 200 g L^{-1} of zinc dust inorder to remove the corrosion products, dried in acetone and noted the weight loss. The percentage inhibitor efficiency was calculated according to the reported method (Negm and Zaki, 2008; Ouf et al., 2010).

2.6.2. Open circuit potential (OCP) measurements

The potential were measured for 15 days under open circuit condition as a function of time against a saturated calomel electrode. All mild steel coupons were prepared and immersed in the cell. The potential values were measured without any disturbance to the coupons. The electrolytes were kept under stagnant condition.

3. Results and discussion

3.1. Structure of the ligand

Condensation of istain monohydrazone with 2-hydroxyacetophenone occurred in 1:1 M ratio to form a bishydrazone, *viz. [(2-hydroxyacetophenone)-3-isatin]-bishydrazone*. Elemental analysis data and other details of the ligand are given in Table 1. The purity of the ligand was checked by TLC technique (silica gel). The electronic spectrum of the ligand show bands at 332 and 310 nm assignable to the n–π^* transitions of the ketimine and aldimine moieties, respectively. Infrared spectrum of the ligand exhibit a broad band at 3357 cm^{-1}, which can be attributed to the hydrogen bonded OH group of the acetophenone moiety. A medium intensity band at 3156 cm^{-1} is due to the N–H vibrations of the indole ring and the strong band at 1687 cm^{-1} may be assigned to ν(C═O) of isatin moiety. Vibrational characteristics of ketimine and aldimine group bands are observed at 1588 and 1551 cm^{-1}, respectively. The bands observed at 1247 and 982 cm^{-1} corresponds to the phenolic (C–O) and (N–N) stretching vibrations, respectively (Nakamoto, 1986). In agreement with the UV–Vis and IR spectral data, the ^{1}H NMR spectrum of the free ligand (Fig. 1) recorded in DMSO-d_6 solution show a signal at 10.69 ppm, characteristic of intramolecular hydrogen bonded –OH proton (Mohanan and Murukan, 2005; Alyea and Malek, 1975). Signals appearing at 9.56 ppm can be attributed to the N–H proton of the indole ring. Aromatic proton signals are observed as multiplet in the range 6.84–7.37 ppm. The mass spectrum of the ligand (Fig. 2) shows the molecular ion peak at *m/z* 279 which is equivalent to the molecular formula of the ligand. The fragmentation peaks are observed at *m/z* 134, 159 and 186 corresponds to (C_8H_8NO), ($C_8H_5N_3O$) and ($C_{10}H_8N_3O$), respectively. The observed peaks are in good agreement with their empirical formula as obtained from elemental analysis data. On the basis of above spectral results, the structure as in Fig. 3 has been assigned for the ligand.

3.2. Structure of the metal complexes

The manganese(II) and cobalt(II) complexes were prepared by treating in 1:2 M ratio of metal salt and ligand, while the other complexes were prepared in 1:1 M ratio. Formation of the metal complexes can be represented by the following general equations.

Table 1 Analytical data and other details of ligand and its metal complexes.

Compound	Molecular formula	Yield (%)	Elemental analysis Found (Calcd.) (%)				Ωm (Ω^{-1} cm^2 mol^{-1})	μ_{eff} (BM)
			C	H	N	M		
L	$C_{16}H_{13}N_3O_2$	83	68.25 (68.82)	4.58 (4.66)	15.18 ((15.05)	–	–	–
[MnL_2]	$C_{32}H_{24}N_6O_4Mn$	79	62.35 (62.84)	3.60 (3.92)	13.83 13.75)	9.12 (8.99)	5.7	5.85
[CoL_2]	$C_{32}H_{24}N_6O_4Co$	87	62.75 (62.45)	3.7 (3.9)	13.76 (13.66)	9.38 (9.58)	9.4	4.80
[NiLCl]	$C_{16}H_{12}N_3O_2Ni$	90	50.94 (51.6)	3.13 (3.22)	11.02 (11.28)	15.25 (15.77)	8.2	D
[CuLCl]	$C_{16}H_{12}N_3O_2Cu$	82	50.25 (50.92)	3.0 (3.2)	10.85 (11.14)	16.40 (16.85)	7.5	1.80
[ZnLCl]	$C_{16}H_{12}N_3O_2Zn$	81	50.18 (50.68)	3.07 (3.17)	10.89 (11.08)	17.05 (17.25)	8.6	D

D – Diamagnetic.

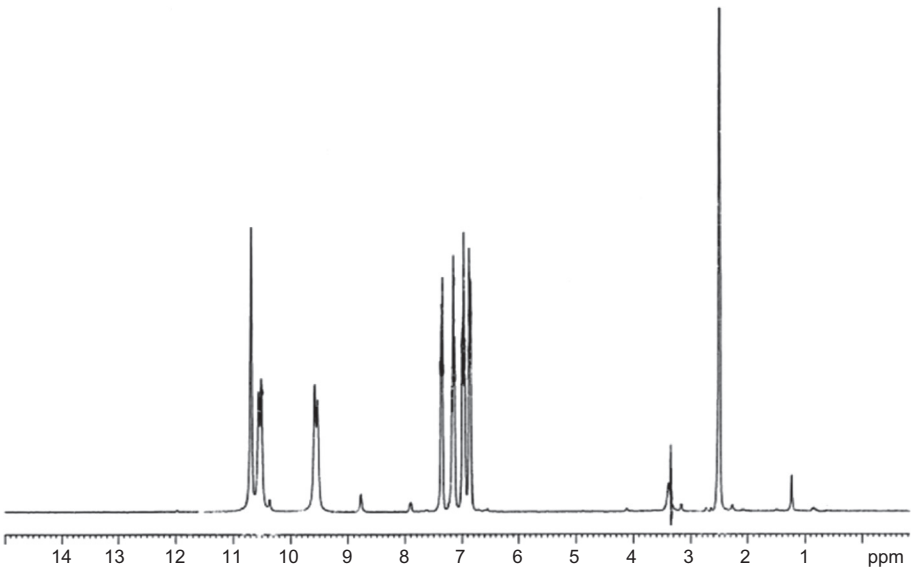

Figure 1 The ^{1}H NMR spectrum of the ligand.

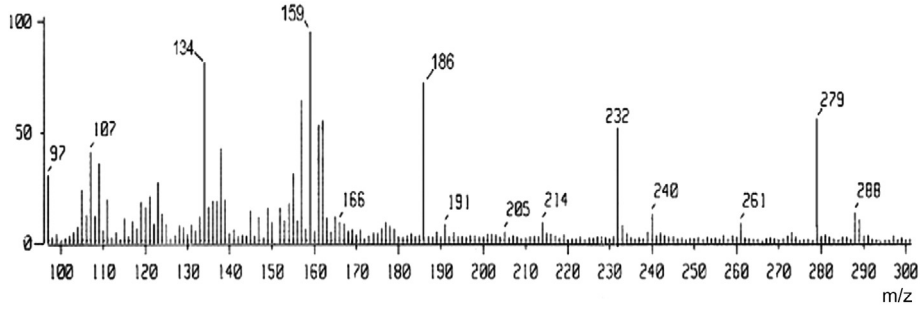

Figure 2 Mass spectrum of the ligand.

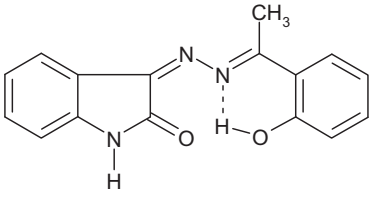

Figure 3 The proposed structure of the ligand.

$MX_2 + L \rightarrow [MLX] + HX;$

where M = Cu(II), Ni(II), Zn(II) and X = Cl^{-}.

$MX_2 + 2L \rightarrow [ML_2] + 2HX;$

where M = Mn(II), Co(II); X = Cl^{-}, CH_3COO^{-}, and L = *[(2-hydroxyacetophenone)-3-isatin]-bishydrazone*.

All complexes are non-hygroscopic solids insoluble in common organic solvents such as benzene, chloroform, carbon tetrachloride and toluene; but soluble in DMSO and DMF. Analytical data of the complexes presented in Table 1 are in good agreement with the theoretical values. The low molar conductance (Table 1) values of the metal complexes in DMSO indicate their non-electrolytic nature (Geary, 1971).

3.2.1. Infrared spectra

The IR spectral bands of the ligand and its metal complexes are given in Table 2 along with the tentative assignments. The internally hydrogen bonded –OH band disappear in the spectra of the metal complexes, indicating the deprotonation and formation of metal–oxygen bond. This is further supported by the shifting of phenolic ν(C–O) towards higher frequency by $\sim$40 cm^{-1}, indicating the coordination of the phenolate oxygen to metal ion (Murukan et al., 2007; Keskioglu et al., 2008). The ν(C=N) vibration of the ligand occurs at 1551 cm^{-1}, which is shifted to a lower frequency by about 20–25 cm^{-1} in the complexes, indicating the involvement of the azomethine nitrogen in chelation with the metal ion. The band corresponding to ν(C=O) at 1687 cm^{-1} is shifted to a lower frequency by about 30–40 cm^{-1}, supporting the coordination of the carbonyl oxygen. However vibrational characteristics of the ring ν(N–H) and ν(C=N) of the ketimine moiety remain almost unaffected, indicating the non participation of these groups in coordination. The bands in the regions 540–550, 450–460, and 350–360 cm^{-1} are ascribed to ν(M–O), ν(M–N), and ν(M–Cl) vibrations, respectively (Ferraro, 1971; Raju and Radhakrishnan, 2003). From the above observations, it can be concluded that the ligand binds to the metal ion in a tridentate fashion through the deprotonated phenolate oxygen,

Table 2 IR spectral bands of the ligand and its metal complexes (cm^{-1}).

L	$[MnL_2]$	$[CoL_2]$	[NiLCl]	[CuLCl]	[ZnLCl]	Tentative assignments
3357	–	–	–	–	–	Hydrogen bonded OH group
3156	3158	3154	3158	3156	3159	Indole ring NH
1687	1657	1658	1658	1657	1656	ν(C═O) ring
1588	1586	1588	1587	1586	1588	ν(C═N) ring
1551	1533	1529	1530	1527	1530	ν(C═N) aldimine
1247	1285	1283	1282	1284	1285	*ν*(C–O) phenolic
982	997	996	997	994	995	*ν*(N–N)
–	461	457	453	456	457	*ν*(M–N)
–	550	551	543	547	542	*ν*(M–O)
–	–	–	355	357	356	*ν*(M–Cl)

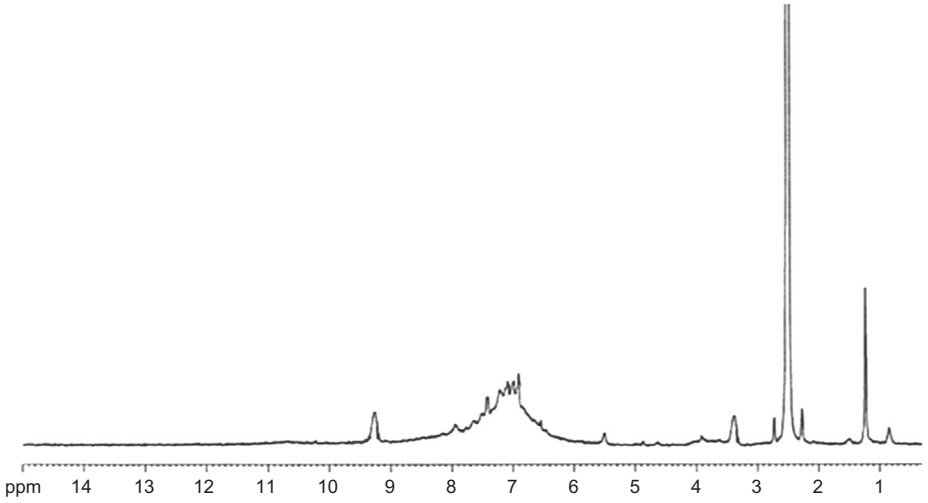

Figure 4 ^1H NMR spectrum of [ZnLCl] complex.

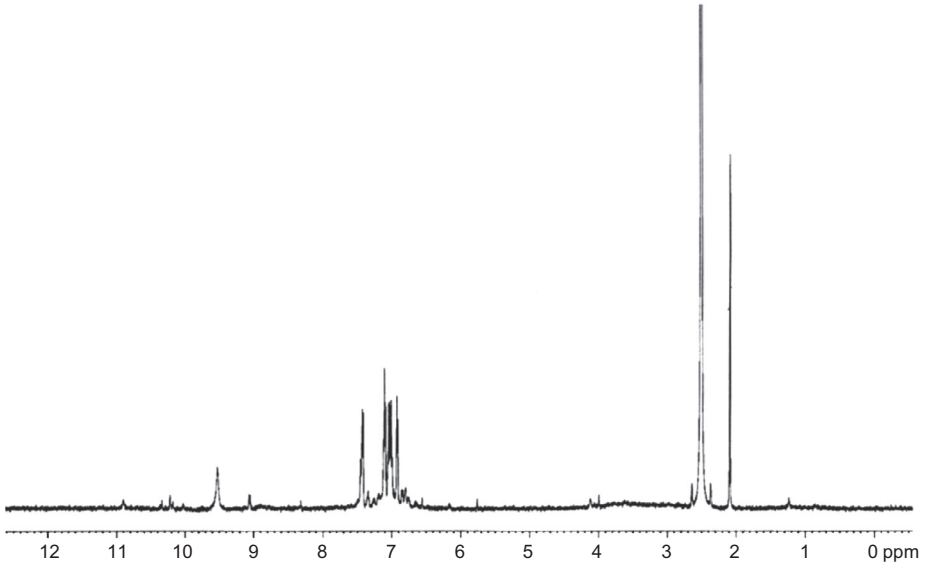

Figure 5 ^1H NMR spectrum of [NiLCl] complex.

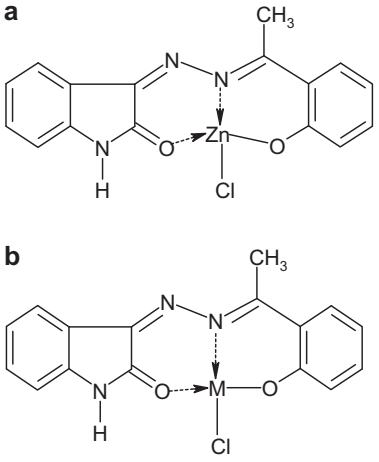

M = Ni(II) and Cu(II)

Figure 6 Proposed structure of (1:1) metal complexes (a) tetrahedral geometry (b) square planar geometry.

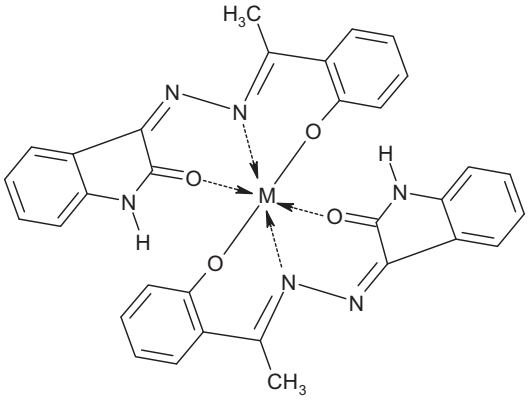

M= Co(II) and Mn(II)

Figure 7 Proposed structure of (1:2) metal complexes (octahedral).

aldimine nitrogen and the carbonyl oxygen of the isatin moiety.

3.2.2. Proton NMR and mass spectra

The spectra of zinc(II) and nickel(II) complexes recorded in DMSO-d_6 are shown in Figs. 4 and 5. The signal at 10.69 ppm in the ^{1}H NMR spectrum of the ligand due to –OH proton, disappeared in the spectrum of both the complexes. This is a clear indication that the phenolate group is coordinated to the metal ion through the phenolate oxygen after deprotonation. On comparing the position of other proton signals in the complexes with those of the ligand signals, it can be concluded that these signals are in the expected region and shift only slightly due to the coordination of the ligand to the metal ion.

The mass spectrum of nickel(II) complex shows a molecular ion peak at m/z = 372.19, which corresponds to [$NiC_{16}H_{12}N_3O_2Cl$] complex. Also it exhibited the significant peaks at m/z 337 and 278 corresponding to [$NiC_{16}H_{12}N_3O_2$] and ($C_{16}H_{12}N_3O_2$), due to the loss of chloride ion and demetallation of the complex, respectively.

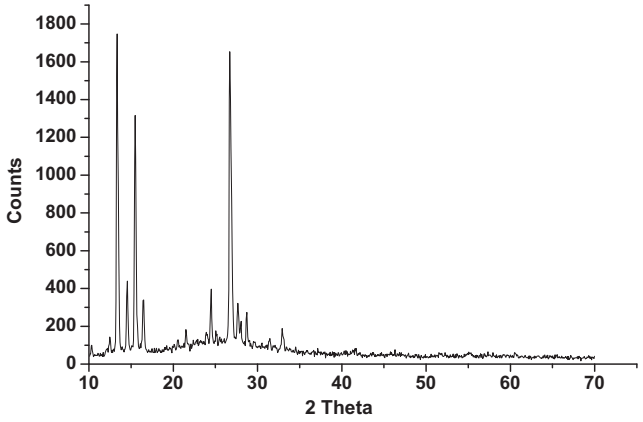

Figure 8 Powder XRD pattern of ligand.

3.2.3. Electronic spectra and magnetic measurements

The electronic spectrum of manganese(II) complex show three peaks at 14,560, 16,400 and 20,000 cm^{-1}, which are assigned to $^6A_{1g} \rightarrow {}^4T_{1g}$, $^6A_{1g} \rightarrow {}^4T_{2g}$ and $^6A_{1g} \rightarrow {}^4E_g$, $^4A_{1g}$ transitions, respectively. These data along with magnetic moment value indicate an octahedral geometry around the metal ion. The cobalt(II) complex exhibits two low level energy bands at 10,760 and 17,600 cm^{-1}, and a high level energy band at 20,500 cm^{-1} which can be assigned to $^4T_{1g}(F) \rightarrow {}^4T_{2g}(F)$, $^4T_{1g}$ $(F) \rightarrow {}^4A_{2g}(F)$ and $^4T_{1g}(F) \rightarrow {}^4T_{2g}(P)$ transitions, respectively, indicating a high-spin octahedral geometry. Cobalt(II) complex display a magnetic moment value of 4.80 BM, which correspond to high-spin octahedral environment around the metal ion (Sathyanarayana, 2001). The nickel(II) complex show three bands at 21,100, 18,240 and 13,700 cm^{-1}, corresponding to $^1A_{1g} \rightarrow {}^1E_g$, $^1A_{1g} \rightarrow {}^1A_{2g}$, and $^1A_{1g} \rightarrow {}^1B_{1g}$ transitions, respectively. These observations and the diamagnetic nature indicate a square planar geometry for this complex (Amirnasr et al., 2006; Kaasjager et al., 2000; Nawar et al., 1990). The copper(II) complex exhibits a broad band centered at 13,660 cm^{-1} due to $^2B_{1g} \rightarrow {}^2A_{1g}$ transition of a distorted square planar geometry. This observation together with the magnetic moment value of 1.80 BM, support a distorted square planar geometry for the copper(II) complex.

On the basis of the analytical data, molar conductance and diamagnetic nature, a tetrahedral geometry is presumed for the zinc(II) complex. It is reported that tetrahedral geometry is the most preferred structure for four coordinated zinc(II) complexes (Dudev and Lim, 2000). From the above spectral data, the structures as in Figs. 6a and b and 7 have been assigned for the metal complexes.

3.2.4. EPR spectrum

The EPR spectrum of the copper(II) complex has been studied in both solid state room temperature and liquid state nitrogen temperature in DMSO solution. At room temperature it shows an intense absorption band in the high field region and is isotropic due to the tumbling motion of the molecules. However, this complex at liquid nitrogen temperature show four well resolved peaks in low field region due to the coupling of the electron spin of the ^{63}Cu nucleus (I = 3/2). The peaks are broad and have the

Table 3 X-ray diffraction data of ligand.

d (Å)	Observed (2θ)	Calculated (2θ)	Observed ($\mathrm{Sin}^2\theta$)	Calculated ($\mathrm{Sin}^2\theta$)	hkl
8.55837	10.32757	9.73037	0.008092	0.007913	011
7.08617	12.48098	12.17608	0.011804	0.011248	110
6.61728	13.36926	13.47934	0.013536	0.013773	101
5.71522	15.49145	15.40634	0.018147	0.017967	111
5.37974	16.46399	16.46116	0.02048	0.020494	102
4.12159	21.54258	21.42414	0.034893	0.034549	121
3.71011	23.96540	24.19917	0.043061	0.043937	201
3.63323	24.48029	24.33162	0.044903	0.044412	210
3.54497	25.09962	25.23564	0.047167	0.047719	113
3.33134	26.73808	27.15036	0.043411	0.055094	202
3.22107	27.67129	27.62343	0.05713	0.056993	213
3.17782	28.05561	28.18538	0.058696	0.059288	212
3.10574	28.72053	28.52983	0.061452	0.060712	221
2.84340	31.43576	31.50199	0.073315	0.073689	203

Table 4 X-ray diffraction data of [NiLCl] complex.

d (Å)	Observed (2θ)	Calculated (2θ)	Observed ($\mathrm{Sin}^2\theta$)	Calculated ($\mathrm{Sin}^2\theta$)	hkl
7.38414	11.97546	11.61971	0.010871	0.010247	110
5.54523	15.96938	15.46919	0.019276	0.018113	111
4.83777	18.3235	18.34401	0.025326	0.025408	200
4.50385	19.69506	19.88048	0.029221	0.029798	112
4.22749	20.99672	21.02052	0.033166	0.033274	210
3.80078	23.38556	23.48189	0.041320	0.041407	103
3.61505	24.60533	25.05360	0.045356	0.047044	220
3.38575	26.30063	26.72082	0.051708	0.053396	122
3.09887	28.78561	28.54213	0.061725	0.060767	221
2.94535	30.32103	38.30608	0.068327	0.068329	213
2.82156	31.68552	31.22965	0.074454	0.072452	222
2.62926	34.07098	34.18252	0.085743	0.086374	203

appearance of ill-resolved triplets. The triplet appearance of the peaks can be attributed to hyperfine splitting of the nitrogen atom ($I = 1$) of the ligand (Mac Donald et al., 1982). The liquid nitrogen temperature in DMSO solution of the complex possesses well-resolved $g_{\|}$ and $g_{\perp}$ regions. The various spin Hamiltonian parameters computed are $g_{\|} = 2.237$, $g_{\perp} = 2.064$, $A_{\|} = 164$ and $A_{\perp} = 50$. Also the trend $g_{\|} > g_{\perp} > g_e$ observed for this complex indicates the presence of unpaired electron in the $d_{x^2-y^2}$ orbital. The covalency parameter (α^2) has been calculated using Kivelson and Nieman equation (Kivelson and Niemann, 1961). The α^2 value (0.76) gives adequate support to the covalent character of the metal–ligand bond.

3.2.5. Powder XRD

The XRD pattern of the ligand (Fig. 8) shows 14 reflections between 2θ ranging from 8° to 32° with maxima at $2\theta = 10.3275°$ corresponding to interplanar distance $d = 8.5583$ Å. The XRD patterns of the ligand (Table 3) and the nickel(II) complex (Table 4) indicate their crystalline nature. A comparison of these values reveal good agreement between calculated and observed values of $\mathrm{Sin}^2\theta$ and 2θ. The ligand is successfully indexed to orthorhombic crystal system with the lattice constant parameters, $a = 12.6263$ Å, $b = 7.6789$ Å, $c = 11.889$ Å and unit cell volume of 1152.7 Å^3 (Eye and Wait, 1960). The diffraction pattern of nickel(II) complex (Fig. 9) shows 12 reflections between 2θ ranging from 10° to 35°. The maxima of 2θ is observed at 11.9754°, with a d-spacing of 7.3841 Å. The $\mathrm{Sin}^2\theta$ and 2θ values have been compared with the calculated ones for identifying the main peaks. The observed values fit well for nickel(II) complex with the lattice parameters, $a = 12.3377$ Å, $b = 9.6612$ Å, $c = 8.6818$ Å corresponding to orthorhombic crystal system. The unit cell volume is calculated to be 1034.8 Å^3.

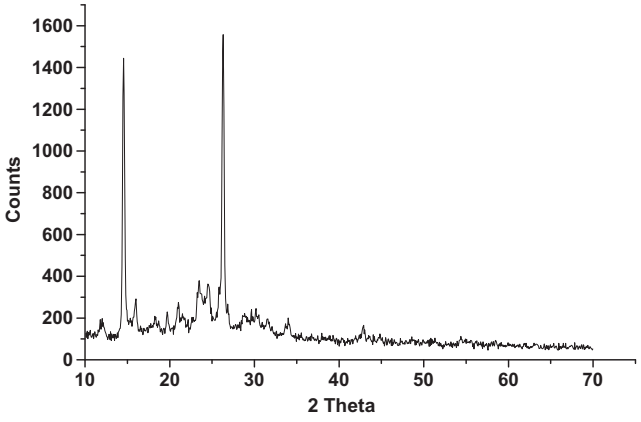

Figure 9 Powder XRD pattern of [NiLCl] complex.

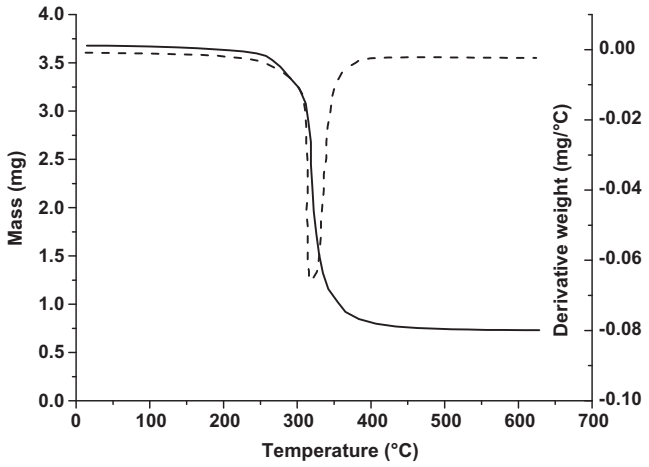

Figure 10 TGA profile of [NiLCl] complex.

3.2.6. Thermogravimetric analysis

The nickel(II) complex is subjected to thermogravimetric analysis in dynamic air in 50–800 °C temperature range, at a heating rate of 10 °C/min. The complex (Fig. 10) is stable up to 240 °C and exhibits a single stage decomposition pattern, as is evident from the DTG profile. The mass loss in the single stage decomposition is in the range of 240–390 °C with maximum peak at 335 °C, which can be attributed to the loss of ligand moiety and its oxidative degradation to metal oxide, above 390 °C. The single stage decomposition of the metal complex usually occur when there is a high degree of electron delocalization along a conjugated system which leads to uniformity in bond strength (Andjelcovie et al., 2001).

3.2.7. Antimicrobial activity

The *in vitro* antimicrobial activity value of the compounds against the growth of micro-organisms is summarized in Table 5. Inhibition is found to increase with increase in concentration of metal complex. The results show that the metal complexes exhibit higher activity against each class of organism. The activity is related to the nature and structure of the complexes. However, all the complexes show higher activity against *E. coli* as compared to *S. typhi* and *S. aureus*. Antibacterial activity can be ordered as [CuLCl] > [NiLCl] > [MnL_2] > [ZnLCl] > [CoL_2] > L. These complexes do not show strong concentration dependence of antimicrobial activity as compared to antifungal activities of the same complexes. The relation between chelation and toxicity is very complex, expected to be a function of steric, electronic and pharmakinetic factors along with mechanistic pathways. The antifungal activity is enhanced several times when the compound is coordinated with metal. The activity of these complexes and ligand follows the order; Cu(II) > Ni(II) > Co(II) > Mn(II) > Zn(II) > L. Comparison of activities shows that the copper complex is more active than the ligand against *R. stolonifer*. The MIC values of some compounds, show significant activity against selected bacterial and fungi species. The results indicate that, these compounds are active in inhibiting the growth of the bacterial and fungal species. A comparative study of the ligand and its complexes indicate that the metal complex exhibit higher antimicrobial activity than the free ligand. Such increased activity of the complexes can be explained on the basis of the Overtone concept and the Tweedy chelation theory (Thimmaiah et al., 1985; Kulkarni et al., 2009). According to the Overtone concept of cell permeability, the lipid membrane surrounding the cell favours the passage of only lipid-soluble materials, due to which liposolubility is an important factor controlling the antimicrobial

Table 5 Antibacterial and antifungal results of the investigated compounds.

Compound	Conc. (μg/ml)	Diameter of zones showing complete inhibition of growth (mm)				
		E. coli	*S. typhi*	*S. aureus*	*R. stolonifer*	*C. albicans*
L	50	5	4	4	3	2
	100	7	6	6	3	3
	200	9	7	5	5	4
[MnL_2]	50	13	12	10	5	4
	100	17	15	14	6	5
	200	19	18	17	8	7
[CoL_2]	50	11	9	8	7	6
	100	13	11	9	9	8
	200	16	14	13	10	9
[NiLCl]	50	16	12	11	8	7
	100	20	17	16	10	9
	200	23	22	21	12	10
[CuLCl]	50	18	16	15	9	8
	100	23	20	18	11	9
	200	30	28	27	13	11
[ZnLCl]	50	12	11	10	3	2
	100	15	14	12	5	4
	200	17	16	15	7	6
Streptomycin[a]	100	30	31	32	-	-
Nystatin[a]	100	–	–	–	35	33

Antibacterial activity: > 15 mm, significant; 10–14 mm, moderate activity; < 10, weak activity. Antifungal activity: > 10 mm, significant activity; 9–7 mm, moderate activity; < 7, weak activity.

[a] Standards.

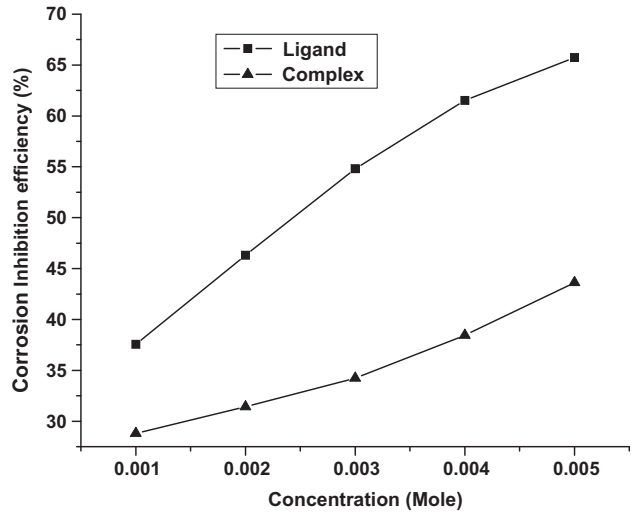

Figure 11 The effect of concentration on corrosion inhibition efficiency of the ligand and its [NiLCl] complex.

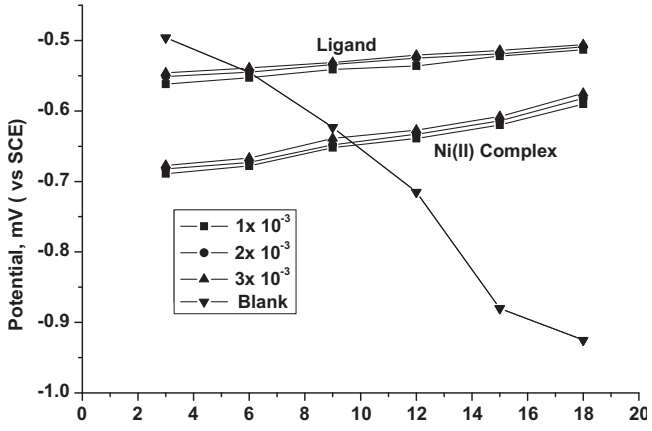

Figure 12 Trend of open circuit potential decay for mild steel immersed in blank and inhibitor solutions.

activity. On chelation, the polarity of the metal ion will be reduced to a greater extent due to the overlap of the ligand orbital and partial sharing of the positive charge of the metal ion with donor groups. Furthermore, the mode of action of the compound may involve formation of a hydrogen bond through the azomethine group with the active centre of cell constituents, resulting in interference with normal cell processes.

3.2.8. Corrosion inhibition efficiency

The effect of concentration on the inhibition efficiency of the ligand and its nickel(II) complex are shown in Fig. 11. Corrosion inhibition is attributed to the adsorption of inhibitors on mild steel. The weight loss of mild steel immersed in 1 M H_2SO_4 for 15 days with and without the corrodent-inhibitor of varying concentration from 1×10^{-3} g to 5×10^{-3} g is measured and compared. Apart from this, the ligand is found to possess more inhibitory action than the metal complex. The inhibition efficiency increases with increase in concentration of the additives. The lone pair of electrons of nitrogen and oxygen atoms along with the delocalized π-electron can be the reason for higher inhibition efficiency (Sanyal and Kumar, 2010). These factors play the vital role in the adsorption of the inhibitor and the formation of coordinate bond with metal. The adsorption of inhibitor on the mild steel surface can occur either directly by the interactions between the π-electrons of the inhibitor and the vacant d-orbitals of metal surface atoms. The adsorption of inhibitor on mild steel may also be due to the interaction of nitrogen and oxygen with the surface atoms of metal. As inhibitor concentration increases, it covers more and more surface area and results in the reduction of corrosion rate (Hameed et al., 2012). It has been observed that Fig. 12 shows the trend of OCP decay with and without the corrodent inhibitor (Table 6) of varying concentration from 1×10^{-3} g to 5×10^{-3} g for 15 days. The OCP decay of a mild steel coupon kept in a blank cell *i.e.* without inhibitor (1 M H_2SO_4) is also given in Fig. 12 to understand the extent of OCP deviation due to the presence of the inhibitor. In the case of blank solution the initial OCP value instantly changes to a negative value as high as −0.925 mV which shows severe corrosion attack. However the addition of different concentration of the ligand and complex to the solution is able to bring the potential values towards positive region. This is due to the ability of the ligand-complex solution to form a passive film on the surface of mild steel coupons. Extend of film formation is more prominent in the ligand when compared to the complexes because the ligand is more chemical adsorptive than complexes. It can be explained on the basis of the effect of chemical structure. In this respect, the isatin ring, benzene ring, N–H, C═N and C═O of bishydrazone can form a big π bond accordingly, not only the π of benzene, C═O enter unoccupied orbital of iron, but also the π^* orbital can accept the electron of d orbital of iron to form back bonds. These back bonds produce more than one centre of chemical adsorption on the mild steel surfaces (Hameed, 2011). In the case of metal complexes the chemical adsorption is less because the ligand shares its lone pair to the metal ion that will reduce the effective adsorption of mild steel surface.

Table 6 Variation of open circuit potential decay for mild steel immersed in blank and inhibitor solutions.

No. of days	Potential blank (mV)	Potential (mV) of ligand in various conc.			Potential (mV) of complex in various conc.		
		1×10^{-3} (g)	3×10^{-3} (g)	5×10^{-3} (g)	1×10^{-3} (g)	3×10^{-3} (g)	5×10^{-3} (g)
3	−0.496	−0.562	−0.551	−0.546	−0.689	−0.682	−0.677
6	−0.545	−0.553	−0.545	−0.539	−0.678	−0.673	−0.667
9	−0.623	−0.541	−0.534	−0.531	−0.652	−0.648	−0.639
12	−0.715	−0.536	−0.525	−0.521	−0.639	−0.633	−0.627
15	−0.880	−0.522	−0.519	−0.514	−0.620	−0.614	−0.608
18	−0.925	−0.513	−0.509	−0.506	−0.590	−0.582	−0.575

4. Conclusion

The bishydrazone derived from isatin monohydrazone and 2-hydroxyacetophenone acts as monobasic tridentate. On the basis of all the spectral data, it is observed that manganese(II) and cobalt(II) complexes possess an octahedral geometry, nickel(II) complex exhibit square planar geometry, copper(II) complex possess a distorted square planar geometry whereas zinc(II) complex possess a tetrahedral geometry. The XRD studies show that both the ligand and nickel(II) complex possess crystalline nature with orthorhombic crystal lattice. In view of biocidal activity observations of hydrazone derivatives, there is an enhancement in the antimicrobial activity of the complexes when compared to that of ligand. A comparative study of the MIC values of the ligand and its complexes indicate that the copper(II) complex exhibit higher antibacterial/antifungal activity than the other compounds. Corrosion inhibition efficiency of the ligand and its nickel(II) complex reveal that the ligand possess greater activity than the metal complex.

Acknowledgements

We express our sincere thanks to Professor and Head, Department of Chemistry, University of Kerala, Kariavattom Campus, Trivandrum, for providing us with necessary facilities for carrying out this work successfully. Instrumental facilities provided by SAIF Cochin, IIT Bombay, CDRI Lucknow and NIIST Trivandrum are gratefully acknowledged.

References

Alyea, E.C., Malek, A., 1975. Synthesis and characterization of some dibasic tridentate Schiff base ligands. Can. J. Chem. 53, 939–941.

Amirnasr, M., Schenk, K.J., Meghdadi, S., Morshedi, M., 2006. Synthesis, characterization and X-ray crystal structures of [Ni(Me-sal)$_2$dpt] and [Ni(Me-sal)dpt]Cl. Polyhedron 25, 671–677.

Andjelcovie, K., Sumar, M., Ivanovic-Burmazovic, I., 2001. Thermal analysis in structural characterization of hydrazone ligands and their complexes. J. Therm. Anal. Cal. 66, 759–778.

Bauer, A.W., Kirby, W.M.M., Sherries, J.C., Turck, M., 1966. Antibiotic susceptibility testing by standard single disc diffusion method. Am. J. Clin. Pathol. 45, 493–496.

Dudev, T., Lim, C., 2000. Tetrahedral vs. octahedral zinc complexes with ligands of biological interest: a DFT/CDM study. J. Am. Chem. Soc. 122, 11146–11153.

Ercag, A., Yildirim, S.O., Akkurt, M., Ozgar, M.U., Heinemann, F.W., 2006. Novel isatin-Schiff base Cu(II) and Ni(II) complexes. X-ray crystal structure of *bis[3-(4-hexylphenylimino)-1H-indol-2(3H)-one]-dichlorocopper(II)* complex. Chin. Chem. Lett. 17, 243–246.

Eye, R.W.M.D., Wait, E., 1960. X-ray Powder Photography in Inorganic Chemistry. Butterworths, London.

Ferraro, J.R., 1971. Low Frequency Vibrations of Inorganic and Coordination Compounds. Plenum Press, New York.

Geary, W.J., 1971. The use of conductivity measurements in organic solvents for the characterization of coordination compounds. Coord. Chem. Rev. 7, 81–122.

Hameed, R.S.A.E., 2011. Aminolysis of polyethylene terephthalate waste as corrosion inhibitor for carbon steel in HCl corrosive medium. Adv. Appl. Sci. Res. 2, 483–499.

Hameed, R.S.A.E., Shafey, H.I.A., Magd, A.S.A., Shehata, H.A., 2012. Pyrazole derivatives as corrosion inhibitor for C-steel in hydrochloric acid medium. J. Mater. Environ. Sci. 3, 294–305.

Hassan, A.M.A., 1997. Synthesis and characterization of Ni(II), Cr(III), Co(II), Cu(II), Zn(II) and Cd(II) complexes with isatin-isonicotinoyl hydrazone. Indian J. Chem. 36A, 241–245.

Kaasjager, V.E., Puglisi, L., Bouwman, E., Driessen, W.L., Reedijk, J., 2000. Synthesis, characterization and crystal structures of nickel complexes with dissymmetric tetradentate ligands containing a mixed-donor sphere. Inorg. Chim. Acta 310, 183–190.

Keskioglu, E., Gunduzalp, A.B., Cete, S., Hamurcu, F., Erk, B., 2008. Cr(III), Fe(III) and Co(III) complexes of tetradentate (ONNO) Schiff base ligands: synthesis, characterization, properties and biological activity. Spectrochim. Acta A 70, 634–640.

Kivelson, D., Niemann, R., 1961. ESR studies on the bonding in copper complexes. J. Chem. Phys. 35, 149–155.

Kulkarni, A.D., Patil, S.A., Badami, P.S., 2009. Electrochemical properties of some transition metal complexes: synthesis, characterization and In-vitro antimicrobial studies of Co(II), Ni(II), Cu(II), Mn(II) and Fe(III) complexes. Int. J. Electrochem. Sci. 4, 717–729.

Mac Donald, L.G., Brown, D.H., Smith, W.E., 1982. The electron spin resonance of Cu(II) Schiff base complexes containing amino acids as part of the ligand. Inorg. Chim. Acta 63, 213–216.

Mariar, C.R., Belicchi, F.M., Franco, B., Corrado, P., Giorgio, P., Silvana, P., Monica, S., 2004. Synthesis, characterization and biological activity of Ni(II), Cu(II) and Zn(II) complexes of isatin hydrazones. J. Inorg. Biochem. 98, 313–321.

Mohanan, K., Murukan, B., 2005. Complexes of Mn(II), Fe(II), Co(II), Ni(II), Cu(II) and Zn(II) with a bishydrazone. Synth. React. Inorg. Met. Org. Chem. 35, 837–844.

Mohanan, K., Thankamony, M., Kumari, B.S., 2008. Synthesis, spectroscopic characterization, and thermal decomposition kinetics of some lanthanide(III) nitrate complexes of 2-(N-o-hydroxyacetophenone)amino-3-carboxyethyl 4,5,6,7-tetrahydrobenzo[b]thiophene. J. Rare Earths 26, 463–470.

Murukan, B., Mohanan, K., 2007. Synthesis, characterization and antibacterial properties of some trivalent metal complexes with *[(2-hydroxy-1-naphthaldehyde)-3-isatin]-bishydrazon*e. J. Enzyme Inhib. Med. Chem. 22, 65–70.

Murukan, B., Kumari, B.S., Mohanan, K., 2007. Synthesis, spectral, electrochemical and antibacterial studies of Cu(II) complexes with isatin derived bishydrazone and different co-ligands. J. Coord. Chem. 60, 1607–1617.

Nakamoto, K., 1986. Infrared and Raman Spectra of Inorganic and Coordination Compounds. Wiley Interscience, New York.

Nawar, N., Khattab, M.A., Hosny, N.M., 1990. Some metal(II) complexes of o-aminoacetophenone benzoylhydrazone (Aabh): their preparation, characterization and antimicrobial activity. Synth. React. Inorg. Met. Org. Chem. 29, 1365–1384.

Negm, N.A., Zaki, M.F., 2008. Corrosion inhibition efficiency of nonionic Schiff base amphiphiles of p-aminobenzoic acid for aluminum in 4N HCL. Colloids Surf. Physicochem. Eng. Aspects 322, 97–102.

Ouf, A.E.F.M., Ali, M.S., Soliman, M.S., Defrawy, A.M.E., Mostafa, S.I., 2010. Synthesis and characterization of new transition metal complexes of Schiff base derived from 2-aminopyrimidine and 2,4-dihydroxybenzaldehyde and its applications in corrosion inhibition. J. Korean Chem. Soc. 54, 402.

Pandeya, S.N., Sriram, D., Nath, G., De Clercq, E., 1999. Synthesis, antibacterial, antifungal and anti-HIV evaluation of Schiff and Mannich bases of isatin derivatives with 3-amino-2-methylmercapto quinazolin-4(3*H*)-one. Pharm. Acta Helv. 74, 11–17.

Raju, K.C., Radhakrishnan, P.K., 2003. Complexes of Cu(II) with 2,3-dimethyl- 4-formyl-(benzhydrazide)-1-phenyl-3-pyrazolin-5-one. Synth. React. Inorg. Met. Org. Chem. 333, 1307–1318.

Sanyal, S., Kumar, A., 2010. Inhibitive effect of some Schiff base ligands for corrosion of mild steel in acidic media. J. Indian Chem. Soc. 87, 189–194.

Sathyanarayana, D.N., 2001. Electronic Absorption Spectroscopy and Related Techniques. University Press (India) Limited, Hyderabad, India.

Sridhar, S.K., Ramesh, A., 2001. Synthesis and pharmacological activities of hydrazones, Schiff and Mannich bases of isatin derivatives. Biol. Pharm. Bull. 24, 1149–1152.

Sridhar, S.K., Saravanan, M., Ramesh, A., 2001. Synthesis and antibacterial screening of hydrazones, Schiff and Mannich bases of isatin derivatives. Eur. J. Med. Chem. 36, 615–625.

Sridhar, S.K., Pandeya, S.N., Stables, J.P., Ramesh, A., 2002. Anticonvulsant activity of hydrazones, Schiff and Mannich bases of isatin derivatives. Eur. J. Pharm. 16, 129–132.

Thimmaiah, K.N., Lloyd, W.D., Chandrappa, G.T., 1985. Stereochemistry and fungitoxicity of complexes of p-anisaldehydethiosemicarbazone with Mn(II), Fe(II), Co(II) and Ni(II). Inorg. Chim. Acta 106, 81–83.